Exploring Hemodynamics in Subject-Specific Carotid Arteries with MRI-Based CFD Models and Explainable AI

T Raja Rani [1], Mohamed Siraj[2], Woshan Srimal[3], Abdullah Al Shibli[4], Nooh Zayid Suwaid Al Bakri[5] , and T S L Radhika[6]

[1,2,3,4,5] Military Technological College, Muscat, Oman
[6] BITS Pilani, Hyderabad Campus, Hyderabad, India
Corresponding author[1] email: rani.t@mtc.edu.om

Abstract. Investigating the hemodynamics of human carotid arteries involves a detailed examination of blood flow dynamics within the individualized vascular structures on the left and right sides of the neck. This study focuses on exploring and analyzing the unique hemodynamic characteristics of these arteries in a subject-specific context, offering valuable insights into blood circulation patterns and fluid dynamics associated with these vital blood vessels. To achieve this, we developed Computational Fluid Dynamics (CFD) prototypes for both the left and right carotid arteries using MRI scans from an individual. These CFD models were simulated under various physiological conditions, and the generated data were analyzed with machine and deep learning models to understand variations in flow characteristics. The findings revealed statistically significant differences in parameters such as wall shear stress and blood velocity between the two (left-sided and right-sided) arteries. Further analysis identified potential unhealthy conditions in the subject's left carotid artery. The Shapely Additive Explanations (SHAP) analysis gave in-depth knowledge, revealing that blood velocity in the common carotid artery (CCA) is the primary factor affecting blood flow in the internal (ICA) and external carotid arteries (ECA). Higher CCA velocity boosts velocities in the ICA and ECA, while lower CCA velocity reduces them. Additionally, blood velocity and viscosity are the main factors influencing wall shear stress (WSS) in each artery segment, with higher values increasing WSS and lower values reducing it. Other factors, like blood density and reference pressure, have minimal impact on blood flow and WSS.

Keywords: CFD prototype, Subject Specific Artery, Numerical model, Predictive analysis, SHAP

1. Introduction.

The presence of atherosclerosis at the carotid bifurcation represents a significant risk factor for the occurrence of strokes. Atherosclerosis in this crucial arterial junction involves plaque buildup composed of cholesterol, fatty deposits, and inflammatory cells. This accumulation can lead to the narrowing or complete blockage of the carotid arteries, obstructing the normal blood flow to the brain. Consequently, the risk of ischemic stroke significantly increases, as the compromised blood supply may result in insufficient oxygen and nutrients reaching vital brain regions. Managing and addressing atherosclerosis at carotid bifurcation is pivotal in stroke prevention and cardiovascular health.

A few studies on the methodologies adopted by researchers for carotid artery disease identification are as follows: Examining these trends and shifts in methodologies provides valuable insights into the progress of medical research, enabling a comprehensive overview of the tools and approaches. Abdul, Nitesh Kumar, and Raghuvir Pai [1] conducted a Fluid-Structure Interaction (FSI) investigation on two distinct three-dimensional patient-specific scenarios: (a) normal carotid bifurcation and (b) a stenosed carotid bifurcation. They evaluated the hemodynamic parameters under diverse physiological conditions and comprehended the development of atherosclerosis in the carotid artery bifurcation for normal and hypertensive states. In their study on flow dynamics in patient-specific bifurcated carotid arteries, Hedge et al. [2] noted that the wall Shear Stress (WSS) is influenced by artery topology and blood flow characteristics (pulsatile nature and viscosity model), and maximum WSS occurs at locations with flow separation and high-velocity gradients. Their results from Computational Fluid Dynamics (CFD) simulations indicated that the Carreau model exhibits greater sensitivity to WSS compared to the Casson model, especially at higher flow velocities during the systolic phase. A study by Harita and Anburajan [3] outlined the technical aspects of generating patient-specific Computer-

Aided Design (CAD) models of the carotid artery (CA), both with and without plaque. They asserted that utilizing CT image analysis through specialized software enables these CAD models to replicate the patient's conditions accurately. Pinho et al. [4] created a computational model integrating transient carotid artery wall deformation and investigated the impact of artery compliance on WSS. For this, the required data was taken from ultrasound images of two patients, one with mild internal carotid artery (ICA) stenosis and another without visible stenosis. A study by Cui et al. [5] indicated that variations in the geometry and height of the carotid artery bifurcation angle and the carotid internal angle led to distinct patterns of laminar shear stress. Moreover, alterations in the artery bifurcation angle, including size and height, influenced extracellular matrix (ECM) and Yes-associated protein (YAP), resulting in diverse clinical manifestations. Hameed et al. [6] observed transitional flow in the post-stenotic region due to the elevated Reynolds number during peak systole. However, the flow demonstrated laminar characteristics at the peak diastole. They noted that the ICA stenosis induced elevated WSS, erratic flow patterns, and low-pressure regions. Velocity and pressure profiles oscillated in the immediate downstream vicinity of the stenosis. Moreover, they observed that, in the stented model, the flow did not change into the turbulent regime in peak systole and diastole conditions.

Lopes et al. [7] conducted a systematic review to illustrate the methodology employed in modeling, simulating, and analyzing carotid blood flow while identifying potential gaps and challenges within this research field. Their key observations are: (i) Magnetic Resonance and Computed Tomography are the preferred techniques for acquiring images to construct 3D simulation models. (ii) Traditionally, the carotid artery assumes Newtonian blood viscosity. Yet, recent findings revealed substantial differences in computed hemodynamic parameters like WSS between Newtonian and non-Newtonian models, suggesting the importance of considering blood as non-Newtonian. (iii) Laminar flow assumption holds for healthy carotid artery models; however, in severely stenosed geometries, they suggested that careful consideration is needed due to the potential shift of fluid flow to transitional or turbulent. Furthermore, they identified patient-specific simulations of stented arteries as an emerging research avenue, which is crucial for anticipating the hemodynamic impacts of implant devices and potentially refining their design. Considering these observations, it is essential to acknowledge the following works: Mendieta et al. [8] conducted hemodynamic analysis on eight carotid arteries, six from patients with varying degrees of stenosis and two from healthy volunteers, using five viscosity models to assess differences in WSS-based parameters between Newtonian and non-Newtonian models. Their findings suggested that, for image-based computational simulation of atherosclerotic and healthy carotid arteries, the assumption of a Newtonian model is reasonable for OSI (oscillatory shear index) and pressure gradient. Stamou et al. [9] examined the significance of integrating a non-Newtonian model into a plaque deposition framework utilizing near-wall local hemodynamic markers: time-averaged near-wall velocity and the ratio of OSI to WSS. Plaque deposition outcomes were comparable between Newtonian and non-Newtonian simulations, with no more pronounced differences than those among selected markers. More substantial distinctions appeared in hemodynamic properties within the stenosed region, particularly the observation of reduced near-wall reverse flow in non-Newtonian fluid simulations. A study by Kumar et al. [10] focused on a subject-specific case involving partial narrowing of the entire cervical segment of the ICA, with the Common Carotid Artery (CCA) and External Carotid Artery (ECA) appearing normal. The study highlighted that plaque deposition is affected by alterations in lumen diameter and flow recirculation, various hemodynamic parameters, and blood rheology. Furthermore, the Carreau Yasuda model used in their research for evaluating the non-Newtonian properties of blood provided more precise approximations at critical locations than Newtonian properties. Gharahi et al. [11] worked on assessing the impact of various viscosity models on blood flow uncertainty by evaluating axial velocity, WSS, and OSI. Using PC-MRI, they presented a workflow sequence in CFD analysis for a healthy subject. Subsequently, the hemodynamic parameters of a patient with carotid artery stenosis were analyzed. The simulations revealed that the lumped parameter model employed at the outlet produces physiologically reasonable values for hemodynamic parameters. Furthermore, their study observed variations in the dependence of hemodynamic parameters on viscosity models across different geometries.

Furthermore, the distinct anatomical origins of the left and right common carotid arteries are crucial in determining blood flow variations. Studies reported by Sacco et al. [12] showed morphological variations in the internal carotid artery (ICA) distribution based on the side where it is located. The authors

attributed these findings to the anatomical origins of the right and left common carotid arteries, potentially favoring morphological variations in arteries directly originating from the aortic arch. Sabbagh, Essa, and Saleh [13] identified significant variations in the blood flow between right and left common carotid and internal carotid arteries in diabetic and hypertensive patients, notably in the young age group. They observed higher intima-media thickness and lumen diameter values across age groups in the left common carotid artery than in the right. The authors inferred that these anatomical distinctions in the origins of the common carotid artery contributed to different stress levels between the two sides.

As can be seen, there has been limited research on the comprehensive analysis of the subject-specific hemodynamic characteristics of human carotid arteries. This study addresses this gap by developing subject-specific computational fluid dynamics (CFD) models based on MRI scans and analyzing the data using explainable AI techniques. The goal is to provide detailed insights into each artery's unique blood flow patterns and hemodynamic parameters, which could inform personalized medical interventions and improve cardiovascular outcomes. The remainder of the paper is structured as follows: Section II outlines the anatomy of the carotid artery along with the research objectives. Section III elaborates on the methodology, followed by data analysis in Section IV. Concluding remarks and limitations of the study are presented in section V.

II. Problem Statement and Research Objectives

The carotid artery supplies blood to the face, neck, and brain. The primary conduit, known as the CCA, is divided into two branches: the ECA and the ICA, as illustrated in Fig 1. The ECA supplies blood primarily to the face and neck, while the ICA delivers blood to the brain.

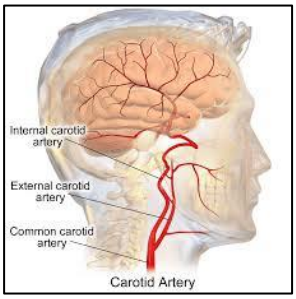

Fig1. Anatomy of Carotid Artery [14, 15]

Thus, studying blood flow in carotid arteries is crucial for assessing brain health, identifying and managing vascular diseases, and minimizing the risk of stroke. As mentioned earlier, this study addresses the challenge of forecasting blood flow dynamics in the subject-specific human carotid artery. We achieved this by creating a prototype of the artery using MRI images of both the left and right arteries (Fig 2).

Left Artery Right Artery

Fig 2. MRI images of subject-specific arteries.

4

These prototypes are imported into CFD software (Fig 3), where simulations are conducted under various physiological conditions to generate a comprehensive dataset.

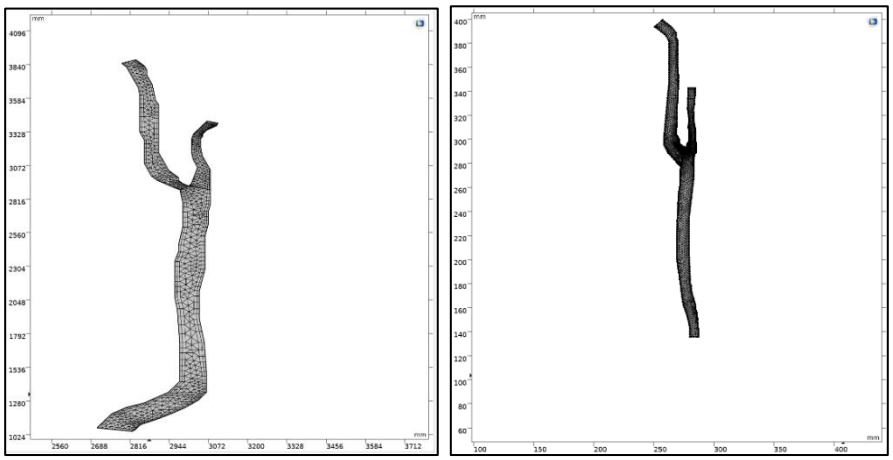

Fig 3. Prototypes created for simulation in COMSOL software.

The research objectives are delineated based on identified gaps in the existing literature. The proposed objectives to analyze the blood flow in the subject-specific carotid artery are as follows:

- Determine an appropriate fluid (blood) model for the problem.
- Identify the most precise ML or DL model for predicting physical quantities such as blood velocity, WSS, and pressure in the three arterial segments.
- Detect anomalies (if any) in an artery.

III. Methodology

The main features of this fluid (blood) flow problem are mathematically described as follows: Blood, acting as the fluid for transportation, is represented as both a Newtonian and a non-Newtonian fluid—specifically, a Casson fluid—while the artery is modeled as a flexible conduit. As mentioned earlier, for simulation, subject-specific prototypes for the left and right carotid arteries are captured from their MRI images and imported into COMSOL Multiphysics, a CFD software. To address the present problem, we adopted the time-independent momentum and continuity equations of incompressible fluids as shown below:

Equation of Continuity:

$$\frac{\partial u}{\partial x} + \frac{\partial v}{\partial y} = 0 \qquad (1)$$

Here *u* and *v* are the fluid velocity components along the *x* and *y* directions respectively.

Equations of Momentum,

$$\rho\left(u\frac{\partial u}{\partial x} + v\frac{\partial u}{\partial y}\right) = -\frac{\partial p}{\partial x} + \left[\frac{\partial}{\partial x}\tau_{xx} + \frac{\partial}{\partial y}\tau_{yx}\right] + \rho g_x \qquad (2)$$

$$\rho\left(u\frac{\partial v}{\partial x} + v\frac{\partial v}{\partial y}\right) = -\frac{\partial p}{\partial y} + \left[\frac{\partial}{\partial x}\tau_{xy} + \frac{\partial}{\partial y}\tau_{yy}\right] + \rho g_y \qquad (3)$$

Where,

$$\tau = 2\,\mu_{app} E \qquad (4)$$

For Newtonian fluid

$$\mu_{app} = \mu \qquad (5)$$

For Casson Papanastasion fluid

$$\mu_{app} = \left[\sqrt{\mu_p} + \sqrt{\frac{\tau_y}{\dot{\gamma}}}\left[1 - exp\left(-\sqrt{m_p\dot{\gamma}}\right)\right]\right]^2 \quad (6)$$

Where,

$$\dot{\gamma} = \frac{1}{2}\left[tr(E^2) - \left(tr(E)\right)^2\right] \quad (7)$$

$$E = \frac{1}{2}\left(\nabla u + (\nabla u)^T\right) \quad (8)$$

Here μ is the viscosity, τ is the deviatoric stress, μ_{app} is the apparent fluid viscosity, μ_p is the plastic viscosity, τ_y is the yield stress, m_p is the model parameter, $\dot{\gamma}$ is the shear rate, and $\dot{\gamma_{ref}}$ is the reference shear rate, and p is the thermodynamic pressure.

These equations are implemented using the laminar flow interface, operating under fully developed flow conditions with the following boundary conditions.

Inlet boundary conditions:

$$u_{av}(x, y) = u_0 \quad (9)$$

Where,

$$u_{av} = -\frac{1}{A}\int_{\partial\Omega_{inf}} u.nds \quad (10)$$

With $A = \int_{\partial\Omega_{iinf}} ds$

Outlet boundary condition:

$$p_{av}(x, y) = p_0 \quad (11)$$

Where,

$$p_{av} = -\frac{1}{A}\int_{\partial\Omega_{out}} pds \quad (12)$$

At the wall, we imposed the no-slip boundary condition given by,

$$u = 0, v = 0 \quad (13)$$

These governing equations, together with the above boundary conditions, are solved using the finite element method (FEM) inbuilt in the COMSOL software. A P1-P1 (linear) finite element discretization is applied to compute velocity and pressure, and the resulting system is solved using the PARDISO solver.

IV. Data Analysis

Data Collection: This section begins with a detailed procedure of the data collection method, followed by the analysis phase.

Firstly, we introduce the dataset, features, and target variables taken for the study. The feature set, consisting of input parameters, includes fluid-related factors (e.g., blood density and viscosity), flow-related variables (such as inlet blood velocity), and material parameters specifying artery characteristics (namely, density, Poisson ratio, and Young's modulus). The target or output variables comprise the crucial physical quantities: WSS, average blood velocity, and average blood pressure. The values for fluid-related parameters are derived from existing data on human blood, while parameters characterizing the elastic behavior of the artery are drawn from anatomical data on the human vascular system. Table 1 shows the complete set of features taken in the study and their permissible values. Specifically, Table 1(b) values are derived from measurements of individual subjects' artery dimensions (Fig 2) utilizing SolidWorks software.

6

Table 1(a). Data on Characteristics of Blood and Carotid Artery [14- 19]

Fluid (blood) Properties		**Both the Artery Properties**	
Density (kg/m^3)	1060	Density	960
Viscosity (Pa. s)	0.004	Young's Modulus (Pa)	490000
		Poisson Ratio	0.45

Table 1(b). Data on Characteristics of Blood and Carotid Artery

Left Artery	**CCA**	**ICA**	**ECA**	**Bifurcation Angle**	**Internal Angle**
Diameter (mm)	5.9	3.9	2.8	39.8°	145.2°
Length (mm)	82.4	52	30		
Right Artery	**CCA**	**ICA**	**ECA**	**Bifurcation Angle**	**Internal Angle**
Diameter (mm)	5.8	3.8	2.9	31°	138.1°
Length (mm)	76.1	58.2	28		

Table 2 presents the data taken to carry out the simulation. For one specific set of parameters, data has been collected in the format shown in Tables 3(a)-3(d) for different mesh settings available in the software.

Mesh Optimization:

Mesh optimization was performed on numerical models designed for the left and right arteries. Results indicated that a NORMAL mesh is optimal for the left artery, while an EXTREMELY FINE mesh is recommended for the right artery for data generation. The normal mesh constituted 1032 triangular and 510 quadrilateral segments, while the extremely fine mesh constituted 4191 triangular and 882 quadrilateral segments. Additional configuration details are shown in Tables 4(a) and 4(b).

Table 2(a). Data on the Newtonian fluid model [14-21]

RPr (mmHg)	**InVel (CCA) (m/s)**	**D (kg/m^3)**	**Vis (Pa. s)**
100	0.351	1060	0.0035
120	0.193	1070	0.004
130	0.1205	1075	0.0045

Table 2(b). Data on Casson fluid model

RPr (mmHg)	**InVel (CCA) (m/s)**	**D (kg/m^3)**	**Vis (Pa. s)**	**Plastic Viscosity**	**Yield stress**	**Model parameter**
100	0.351	1060	0.0035	0.0035	0.0035	50-105
120	0.193	1070	0.004	0.004	0.004	
130	0.1205	1075	0.0045	0.0045	0.0045	
				0..005	0.005	

Table 3(a). Data collection format for Newtonian fluid Model

Vis	In Vel	RefP r	ICA vel	ECA vel	CCA vel	WSS ICA	WSS ECA	WSS CCA	Pr ICA	Pr ECA	Pr CCA

Table 3(b). Description of Entries in Table 3(a)

D	In Vel	Ref Pr	Y_S	Pl_Vis_C	MP_C	D_C	ICA vel	ECA vel	CCA vel	WSS ICA	WSS ECA	WSS ECA	ICA Pr	ECA Pr	CCA Pr

Table 3(c). Data collection format Casson-P Model (Non-Newtonian)

Variable Type	Name	Description	Units	Data type
Input variables (Features)	Vis	Blood viscosity	Pa. s	Numeric
	D	Blood Density	kg/m^3	Numeric
	InVel	Velocity at the CCA entrance	m/s	Numeric
	RPr	Reference Pressure	Pa	Numeric
	Y_S	Yield Stress	Pa	Numeric
	Pl_Vis_C	Plastic Viscosity	Pa. s	Numeric
	MP_C	Model Parameter		Numeric
	D_C	Density Casson	kg/m^3	Numeric
	ICAvel	Blood velocity in ICA	m/s	Numeric
	ECAvel	Blood velocity in ECA	m/s	Numeric
	CCAvel	Blood velocity in CCA	m/s	Numeric
Output variables (Target)	WSSICA	Wall Shear Stress in ICA	Pa	Numeric
	WSSECA	Wall Shear Stress in ECA	Pa	Numeric
	WSSCCA	Wall Shear Stress in CCA	Pa	Numeric
	PrICA	Pressure in ICA	Pa	Numeric
	PrECA	Pressure in ECA	Pa	Numeric
	PrCCA	Pressure in CCA	Pa	Numeric

Table 3(d). Description of Entries in Table 3(c)

Variable Type	Name	Description	Units	Data type
Input variables (Features)	Vis	Blood viscosity	Pa. s	Numeric
	D	Blood Density	kg/m^3	Numeric
	InVel	Velocity at the CCA entrance	m/s	Numeric
	RPr	Reference Pressure	Pa	Numeric
	ICAvel	Blood velocity in ICA	m/s	Numeric
	ECAvel	Blood velocity in ECA	m/s	Numeric
	CCAvel	Blood velocity in CCA	m/s	Numeric
Output variables (Target)	WSSICA	Wall Shear Stress in ICA	Pa	Numeric
	WSSECA	Wall Shear Stress in ECA	Pa	Numeric
	WSSCCA	Wall Shear Stress in CCA	Pa	Numeric
	PrICA	Pressure in ICA	Pa	Numeric
	PrECA	Pressure in ECA	Pa	Numeric
	PrCCA	Pressure in CCA	Pa	Numeric

8

Table 4 (a). Mesh Configuration Left Artery

Number of elements	1542
Number of Vertex elements	124
Number of edge elements	294
Average element quality	0.7762
Minimum element quality	0.1846
Mesh area	253900mm^2

Table 4 (b). Configuration Right Artery

Number of elements	5073
Number of Vertex elements	116
Number of edge elements	510
Average element quality	0.8227
Minimum element quality	0.147
Mesh area	2885mm^2

Moving ahead, these mesh configurations are adopted to generate the data for data analysis. Datasets are generated across diverse flow conditions and fluid properties, ensuring a comprehensive exploration of the blood flow dynamics in the arteries. To identify the optimal fluid model—whether Newtonian or Casson—for blood within these arteries, we assessed WSS, average blood velocity, and blood pressure using both Newtonian and Casson fluid models for each artery.

Statistical Analysis:

A comprehensive statistical analysis assessed potential differences in the data derived from these models. The methodology employed for this investigation is outlined as follows.

1. Assess the normality of the target variable(s) distribution of both fluid models by employing the Anderson-Darling test, which is particularly suitable for unevenly sized samples.
2. If the target variable exhibits normal distribution, conduct the z-test (parametric); otherwise, opt for Dunnett's test.
3. Draw a conclusion based on the obtained p-value, considering its significance in the analysis.

The statistical test details for the target variables in CCA, ICA, and ECA are shown in Table 5. The entry 'No' in the 'Normally Distributed' column signifies a non-normally distributed data distribution. In the 'result' column, 'Yes' and 'No' entries indicate a significant and non-significant difference, respectively, in the distribution of the target variable between the Newtonian and the Casson fluid models.

Table 5. Statistical Analysis at RP 13332.2 Pa

Target Variables	Fluid Model	LEFT Artery			RIGHT Artery		
		Normally Distributed	Dunnett's test		Normally Distributed	Dunnett's test	
			p-value	result		p-value	result
Vel_CCA	Newtonian Casson	No	0.835	No	No	0.834	No
Vel_ICA	Newtonian Casson	No	0.574	No	No	0.574	No
Vel_ECA	Newtonian Casson	No	0.835	No	No	0.191	No
Pr_CCA	Newtonian Casson	No	0.968	No	No	0.370	No
Pr_ICA	Newtonian Casson	No	0.994	No	No	0.577	No
Pr_ECA	Newtonian Casson	No	0.902	No	No	0.541	No
WSS_CCA	Newtonian Casson	No	0.0089	Yes	No	0.1	No
WSS_ICA	Newtonian Casson	No	0.003	Yes	No	0.064	No
WSS_ECA	Newtonian Casson	No	0.058	No	No	0.053	No

Observations:

- Both Newtonian and Casson fluid model predictions on all target variables are significantly different in left and right arteries, which is in tune with the reported in refs [12] and [13].
- No statistically significant difference is evident in the target variables for the right artery. Therefore, we chose to analyze the data produced using the Newtonian model to forecast the target variables for the same.
- Predictions of WSS in CCA and ICA are significantly different for Newtonian and Casson fluid models for the left artery. Based on the statistics shown in Table 6 and the observations noted by Oshinski et al. [16], we opted for the Casson fluid model to predict the target variables in this artery.

Table 6. WSS CCA Data for Left and Right arteries of the models

Artery	Model	Maximum	Mean
Left	Newtonian	0.2658	0.1461
	Casson P	0.3473	0.2042
Right	Newtonian	1.0528	0.5687
	Casson P	1.2281	0.3221

Data Analysis:

The descriptive statistics of the feature set used for the right and left arteries are presented in Tables 7(a) and 7(b).

Table 7(a). Descriptive statistics of data on RIGHT artery

	Vis	D	InVel	RPr
count	192	192	192	192
mean	0.004250	1068.3	0.228250	16332.0
std	0.000560	6.252399	0.094813	1977.02
min	0.003500	1060.0	0.105000	13332.20
25%	0.003875	1060.0	0.158250	15332.15
50%	0.004250	1070.0	0.228500	16665.35
75%	0.004625	0.004625	91.250000	1075.0
max	0.005000	0.005000	105.00000	1075.0

Table 7(b). Descriptive statistics of data on LEFT artery

	YS_C	Pl_Vis_C	MP_C	D_C	Inlet_Vel_C	RPr
count	768	768	768	768	768	768
mean	0.004250	0.004250	77.500000	1068.3	0.228250	16332.0
std	0.000559	0.000559	17.271511	6.24	0.094627	1973.2
min	0.003500	0.003500	50.000000	1060.0	0.105000	13332.2
25%	0.003875	0.003875	63.750000	1060.0	0.158250	15332.2
50%	0.004250	0.004250	77.500000	1070.0	0.228500	16665.4
75%	0.004625	0.004625	91.250000	1075.0	0.298500	17665.2
max	0.005000	0.005000	105.000000	1075.0	0.351000	18665.1

These tables reveal that data has been generated for 192 combinations of features to examine hemodynamics in the left artery, while up to 768 datasets have been generated for the right artery. A snapshot of the velocity and absolute pressure profiles for a specific set of features is presented in Figs 4 and 5.

10

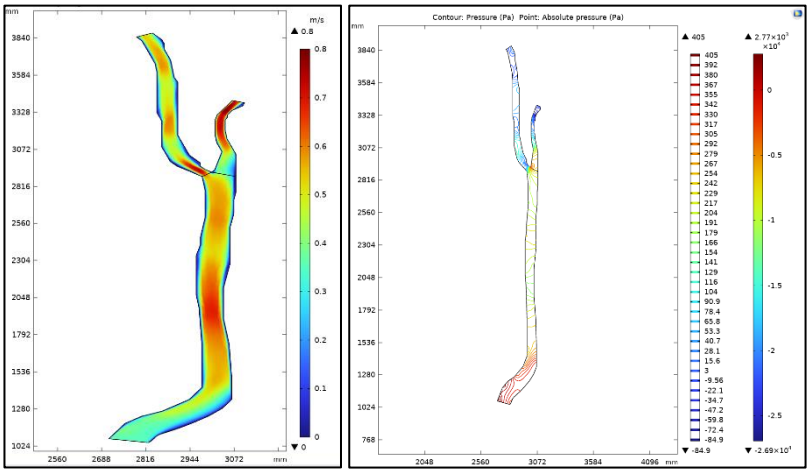

Fig 4. Velocity and Pressure profiles in the Left artery using the Casson fluid model when RPr = 13332.2, InVel = 0.351

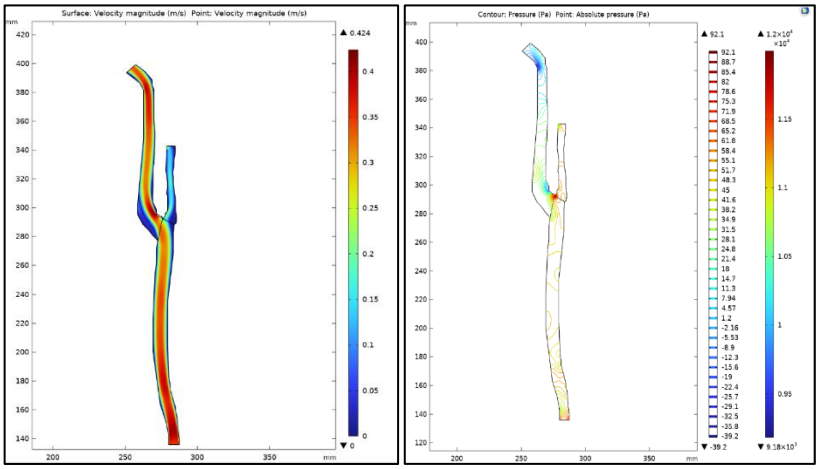

Fig 5. Velocity and Pressure profiles in the Right Artery using the Newtonian fluid model when RPr = 13332.2, InVel = 0.351

Observing these profiles, it becomes evident that the blood velocity in the right artery is lower than in the left. Significantly, the absolute pressure contours in the left artery reveal negative average absolute pressures in the CCA and its bifurcations, suggesting potential abnormalities in its health. Similar trends have been noted for other sets of model parameters. Our next phase involves developing ML and DL models tailored for simulated data. In this stage, we will use the insights and patterns extracted from the data to construct predictive models.

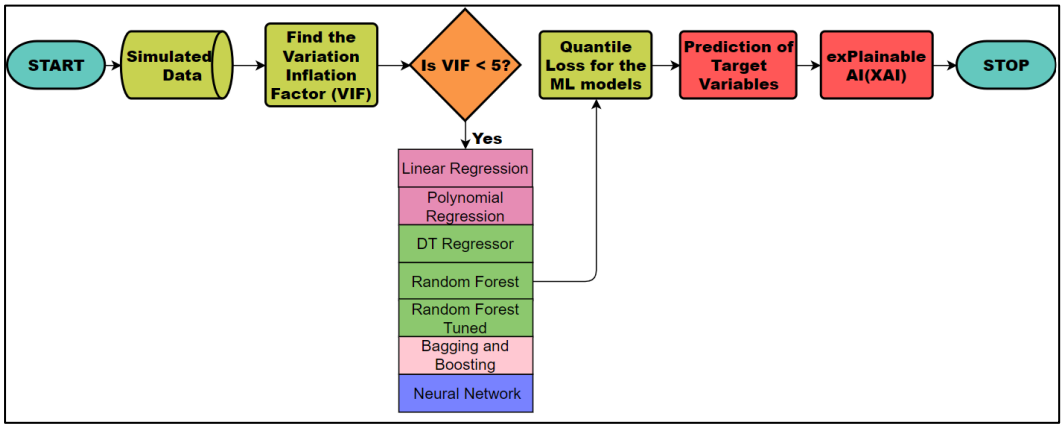

Fig 6. Workflow chart

Fig 6 illustrates the workflow chart for performing data analysis. The simulated data is initially scrutinized to detect correlation within the feature set. Subsequently, feature engineering is carried out to identify an uncorrelated feature dataset for the target variables, as indicated in Table 8.

Table 8. Feature sets and the Target variables

Target Variable	Feature Variable Included	VIF	Feature Variable Excluded	VIF
LAR_ICAvel	YS_C, PlVis_C, MP_C, D_C, CCAvel_C, RPr	>5	D_C	<1.1
LAR_ECAvel	YS_C, PlVis_C, MP_C, D_C, CCAvel_C, RPr	>5	D_C	<1.1
LAR_CCAvel	YS_C, PlVis_C, MP_C, D_C, CCAvel_C, RPr	>5	D_C	<1.1
WSSICA_C	YS_C, PlVis_C, MP_C, D_C, CCAvel_C, RPr	>5	D_C	<1.1
WSSECA_C	YS_C, PlVis_C, MP_C, D_C, CCAvel_C, RPr	>5	D_C	<1.1
WSSCCA_C	YS_C, PlVis_C, MP_C, D_C, CCAvel_C, RPr	>5	D_C	<1.1
RAR_ICAvel	Vis, D, InVel, RPr, CCAvel	>5	InVel	<1.1
RAR_ECAvel	Vis, D, InVel, RPr	<1.1	-	-
RAR_CCAvel	Vis, D, InVel, RPr	<1.1	-	-
WSSCCA	Vis, RPr, CCAvel, InVel, D	>5	InVel	<1.1
WSSECA	Vis, D, RPr, ECAvel, InVel	>5	InVel	<1.1
WSSICA	Vis, D, RPr, ICAvel, InVel	>5	InVel	<1.1

We then analyzed the data using various ML and DL models, linear regression, polynomial, decision tree, random forest, bagging and boosting algorithms, and Neural networks to identify the most suitable model for the simulated data. Based on the performance metrics, MAE (mean absolute error), MPE (mean percentage error), RMSE (Root mean square error), $R^{2,}$ and adjusted R^2, we identified the most accurate ML model for predicting the target variables as presented in Table 9.

12

Table 9. ML model for predicting Target variables.

Target Variable	Best ML Model
LAR_ICA_Vel	Random Forest Tuned
RAR_ICA_Vel	Gradient Boost Regressor
LAR_ECA_Vel	XGBoost Regressor
RAR_ECA_Vel	Gradient Boost Regressor
LAR_CCA_Vel	Random Forest Tuned
RAR_CCA_Vel	Gradient Boost Regressor
LAR_WSS_ICA	Random Forest Tuned
RAR_WSS_ICA	XGBoost Regressor
LAR_WSS_ECA	Random Forest Tuned
RAR_WSS_ECA	XGBoost Regressor
LAR_WSS_CCA	XGBoost Regressor
RAR_WSS_CCA	XGBoost Regressor

Table 10. Optimized values of hyperparameters for target variables in NN models for Left Artery

Target Variable	Batch Size	Epoch
ICA_vel	100	200
ECA_vel	50	60
CCA_vel	100	200
WSSICA	100	200
WSSECA	50	60
WSSCCA	50	60

Table 11. Most reliable ML and NN models for predicting Target variables.

Target Variable	Based on the Quantile Loss Best Model
LAR_ICA_Vel	Neural Network
RAR_ICA_Vel	Linear Regression
LAR_ECA_Vel	Neural Network
RAR_ECA_Vel	Gradient Boost Regressor
LAR_CCA_Vel	XGBoost Regressor
RAR_CCA_Vel	Polynomial Regressor (Degree 4)
LAR_WSS_ICA	Polynomial Regressor (Degree 4) or Neural Network
RAR_WSS_ICA	Polynomial Regressor (Degree 5)
LAR_WSS_ECA	Neural Network
RAR_WSS_ECA	Polynomial Regressor (Degree 5)
LAR_WSS_CCA	Polynomial Regressor (Degree 5)
RAR_WSS_CCA	Polynomial Regressor (Degree 5)

While the Mean Absolute Error (MAE) metric is valuable for evaluating viable regression models, it is crucial to integrate the quantile loss function for a more comprehensive assessment [15]. This approach aids in identifying the most reliable regression models by considering prediction uncertainty, thereby fostering a more robust understanding of their efficacy. Consequently, the final phase of our analysis focuses on quantifying the inherent prediction uncertainty in these models. We investigated the extent of uncertainty surrounding point predictions by employing the Quantile loss function. The quantile loss at 0.1, 0.5, and 0.9 quantiles exhibited an order of magnitude of 10^{-3} for the target variables in the right artery. In contrast, the corresponding quantile losses for the target variables in the left artery were of the order of 10^{-1}. Consequently, neural network (NN) models were constructed for the target variables in the left artery, and we optimized the hyper-parameters presented in Table 10. The quantile losses are visually represented in Figs 7-12, and the most reliable predictor models are presented in Table 11.

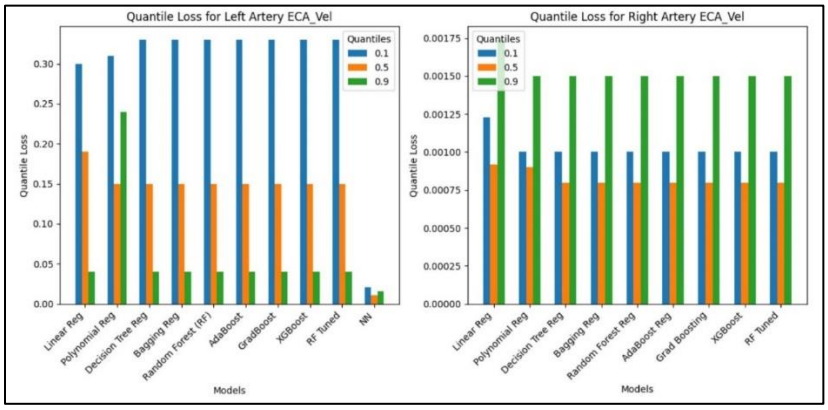

Fig 7. Quantile Loss per quantile for Velocity in ECA of Left & Right Arteries

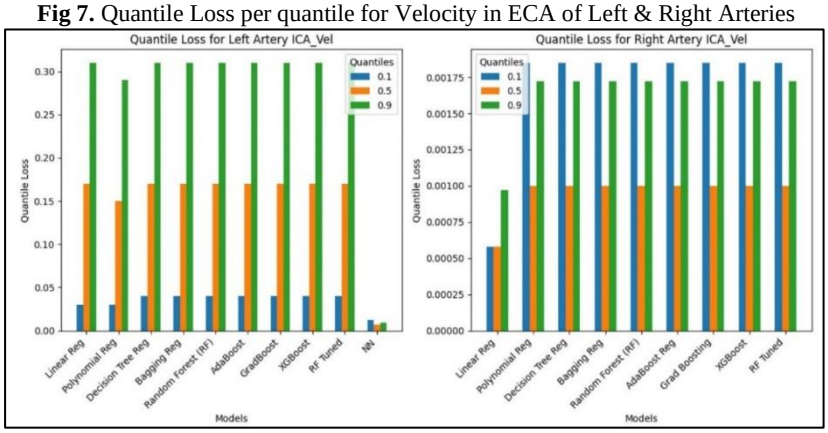

Fig.8. Quantile Loss per quantile for Velocity in ICA of Left & Right Arteries

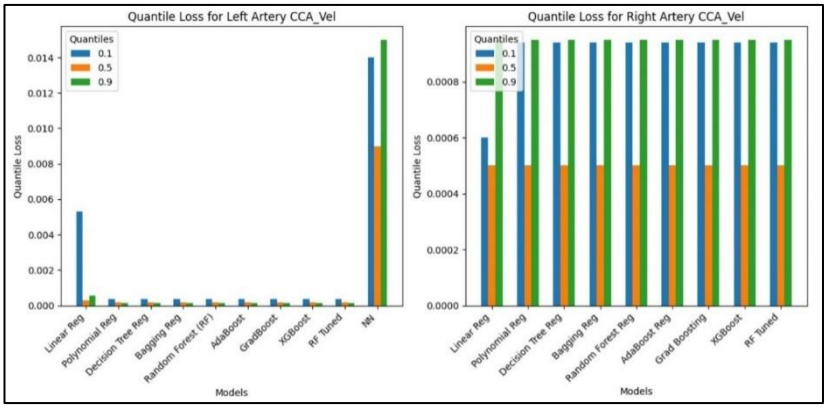

Fig 9. Quantile Loss per quantile for Velocity in CCA of Left & Right Arteries

14

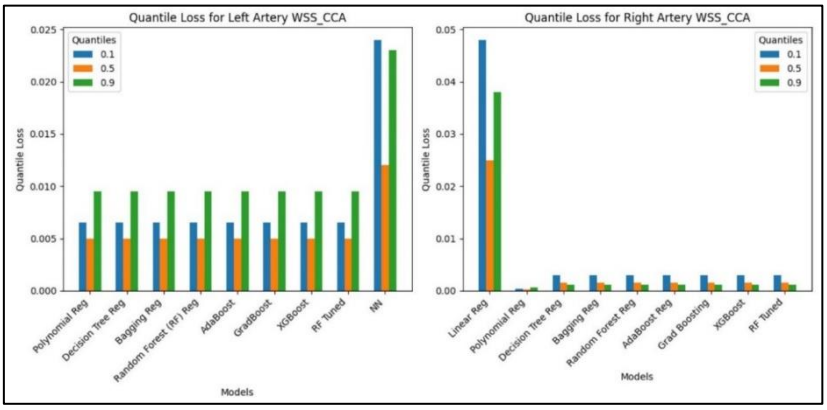

Fig 10. Quantile Loss per quantile for WSS in CCA of Left & Right Artery

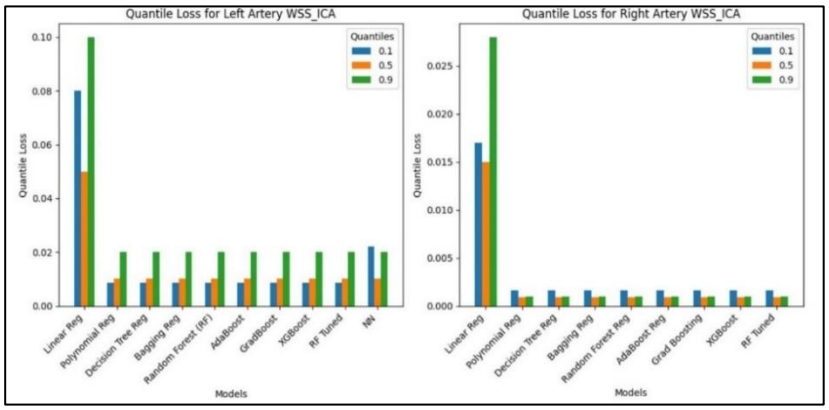

Fig 11. Quantile Loss per quantile for WSS in ICA of Left & Right Arteries

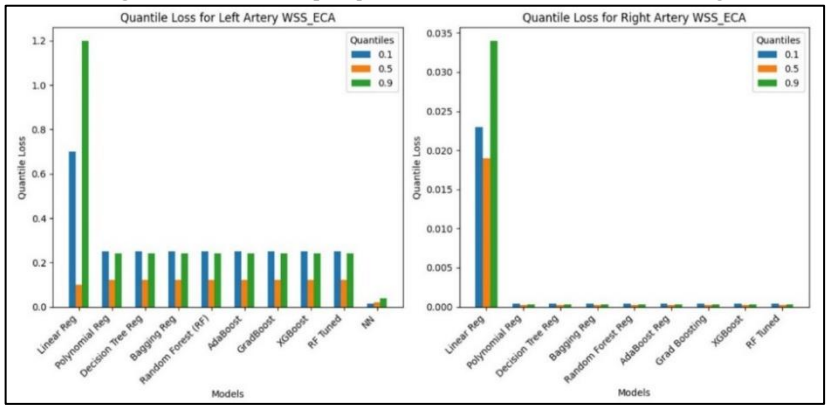

Fig 12. Quantile Loss per quantile for WSS in ECA of Left & Right Arteries

In addition, we identified the most important feature affecting each target variable and presented it in Table 12.

Table 12. Feature importance for target variables

Feature	Left _Casson	Right Newtonian
ICA_Vel	CCA_Vel Pl_Vis	CCA_Vel -
ECA_Vel	CCA_Vel Pl_Vis	CCA_Vel -
WSSICA	ECA_Vel ICA_Vel Pl_Vis	ICA_Vel Viscosity -
WSSECA	ECA_Vel Pl_Vis	ECA_Vel Viscosity
WSSCCA	ECA_Vel Pl_Vis	CCA_Vel Viscosity

Results and Discussion:

To enhance our understanding of how each feature influences the target variables, we employed Shapley Additive exPlanations (SHAP) values in our analysis using the ML algorithms presented in Table 9 for computing SHAP values in each arterial segment.

SHAP analysis of data on the Right artery:

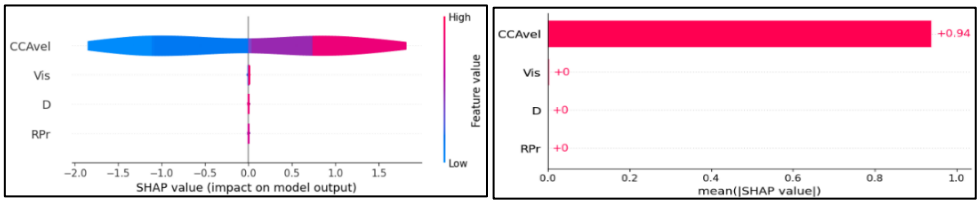

Fig 13. The SHAP and mean SHAP values for the Right artery ECA velocity

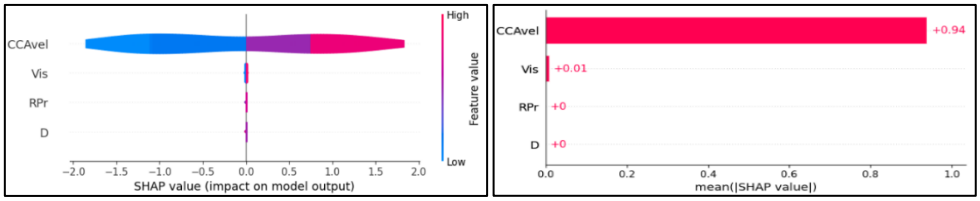

Fig 14. The SHAP and mean SHAP values for the Right artery ICA velocity

Observations:

Significance of CCA velocity: From Figs 13 and 14, SHAP analysis reveals that the most significant factor affecting blood velocity in both ECA and ICA is the blood velocity in the CCA. This implies that changes in blood velocity in the CCA especially impact the velocities in the other segments.

Impact of CCA velocity on bifurcated components: The SHAP analysis further reveals that when the blood velocity in the CCA is higher than the average velocity, it positively affects the velocities in its bifurcated segments (ECA and ICA). Conversely, if the CCA velocity is lower than average, the velocities in these bifurcated segments significantly reduce.

Less significance of other factors: The features- blood viscosity, density, and reference blood pressure are mentioned to have very little significance on the velocities in all three segments (ECA, ICA, and CCA).

16

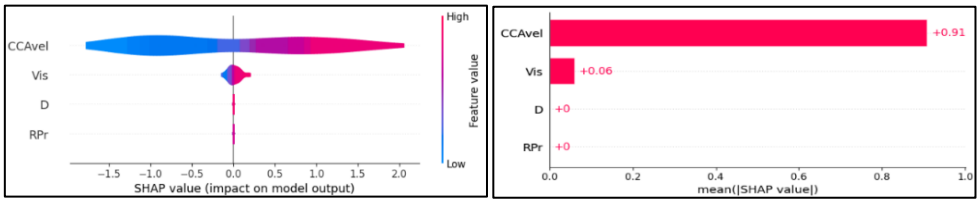

Fig 15. The SHAP and mean SHAP values for the Right artery WSSCCA

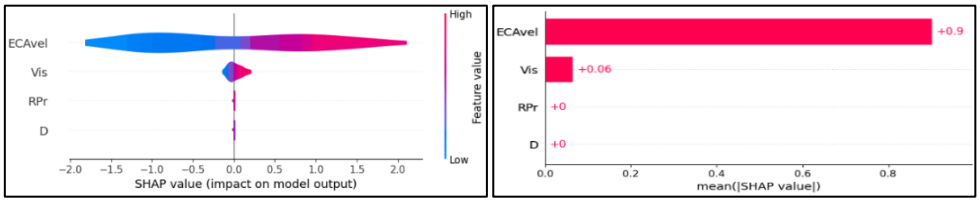

Fig 16. The SHAP and mean SHAP values for the Right artery WSSECA

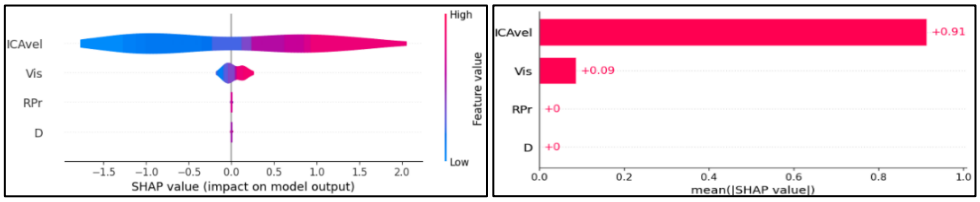

Fig 17. The SHAP and mean SHAP values for the Right artery WSSICA

Observations:

Significance of blood velocities and viscosities: From Figs 15-17, SHAP analysis reveals that the blood velocities in each segment significantly contribute to the WSS experienced in that segment. It also indicates that blood viscosities play a significant role in determining WSS. This implies that changes in blood velocity and viscosity directly influence the magnitude of WSS experienced by the walls of the vessels.

Impact of velocities and viscosities on WSS: When the blood velocities and viscosities are greater than the average values in each segment, they positively impact the WSS. This means that higher velocities and viscosities lead to increased WSS, suggesting a more significant shear force acting on the vessel walls. Conversely, lower blood velocities and low viscosities in the segment are stated to significantly reduce the WSS in them. This indicates that reduced velocities and viscosities result in lower shear stress on the vessel walls.

Limited impact of other features: Features other than blood velocities and viscosities do not affect WSS. This suggests that factors such as blood density, reference blood pressure, or possibly other biological or environmental variables under consideration have negligible influence on the WSS experienced by the vessel walls.

SHAP analysis of data on LEFT artery:

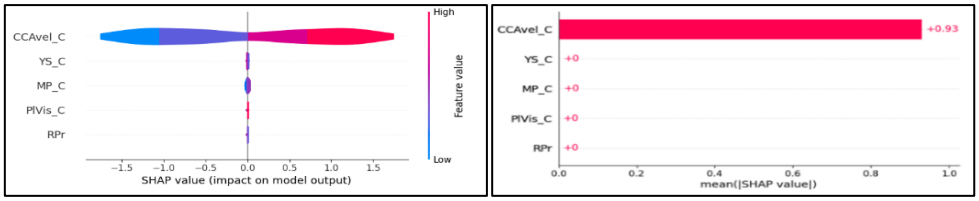

Fig 18. The SHAP and mean SHAP values for the Left artery ECA velocity

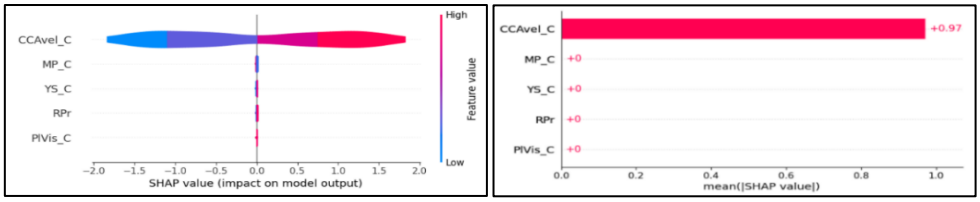

Fig 19. The SHAP and mean SHAP values for the Left artery ICA velocity

Observations:

From Figs 18 and 19, SHAP analysis reveals that the most significant factor affecting blood velocity in both ECA and ICA is the blood velocity in the CCA. Further, when the blood velocity in the CCA is higher than the average velocity, it positively affects the velocities in its bifurcated segments (ECA and ICA). Conversely, if the CCA velocity is lower than average, it significantly reduces the velocities in these bifurcated segments.

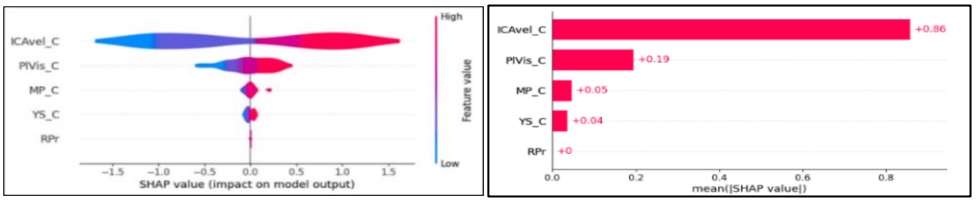

Fig 20. The SHAP and mean SHAP values for the Left artery WSSICA

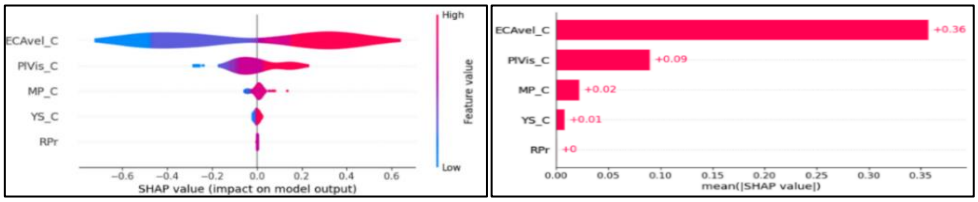

Fig 21. The SHAP and mean SHAP values for the Left artery WSSCCA

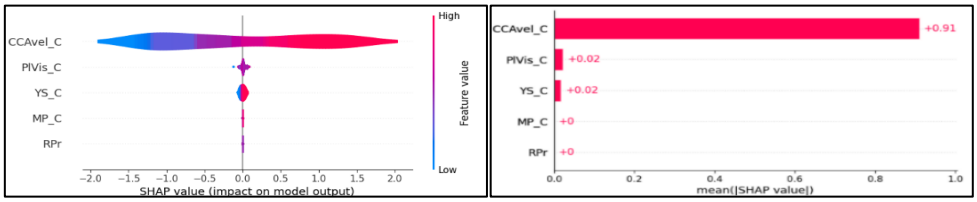

Fig 22. The SHAP and mean SHAP values for the Left artery WSSECA

Observations:

From Figs 20-22, SHAP analysis reveals that the blood velocities in each segment significantly contribute to the WSS experienced in that segment. Additionally, it indicates that blood viscosities also play a significant role in determining WSS, the predominant effect on the WSS in ICA and ECA.

Conclusions

This study investigated the distinct hemodynamic properties of the carotid arteries of a subject-specific data, providing insights into blood circulation and fluid dynamics in these critical vessels. To achieve this, we developed Computational Fluid Dynamics (CFD) models of the left and right carotid arteries using MRI scans from a single individual. These models were simulated under various physiological conditions, with the resulting data analyzed using machine and deep learning techniques to capture differences in flow characteristics. Results showed significant differences in parameters like wall shear stress(WSS) and blood velocity between the left and right arteries. Further analysis indicated potential health risks in the left carotid artery. The SHAP analysis revealed that blood velocity in the common carotid artery (CCA) is the dominant factor influencing blood flow in the internal (ICA) and external carotid arteries (ECA). When the blood velocity in

18
the CCA is high, it increases the flow in both the ICA and ECA. Conversely, lower blood velocities in the CCA result in decreased flow in the ICA and ECA. Blood velocity and viscosity are the main factors impacting WSS in each artery segment, with higher values elevating WSS and lower values reducing it. Other variables, such as blood density and reference pressure, have minimal influence on blood flow and WSS.

Funding: This research received no specific grant from any funding agency.

Disclosure of potential conflicts of interest: The authors declared no conflict of interest.

Data Availability Statements: The data that support the findings of this study are not openly available due to reasons of sensitivity and are available from the corresponding author upon reasonable request. Data are in controlled access data storage at Military Technological College, Muscat, Oman.

References

1. Abdul Khader, S.M., Nitesh Kumar, and Raghuvir Pai, Fluid-Structure Interaction Study of Stenosed Carotid Artery Considering the Effects of Blood Pressure and Altered Gravity, Finite Element Methods and Their Applications. Intech Open, 2021. doi:10.5772/intechopen.93908.
2. Hegde, Abhimanyu H. and Bhat, Shreyas kumar R. and L, Rakesh and K, Prakashini, A Computational Fluid Dynamics Study on Patient-Specific Bifurcated Carotid Artery, Engineered Science, 2022, 19, 243-252.
3. K. Harita and M. Anburajan, Patient-specific CAD model of useful carotid artery (CA) for CFD analysis of CA with plaque condition, 2013 International Conference on Communication and Signal Processing, Melmaruvathur, India, 2013, 377-381.
4. Pinho, N. et al., Patient-Specific Study of a Stenosed Carotid Artery Bifurcation Using Fluid–Structure Interactive Simulation. In: Tavares, J., Natal Jorge, R. (eds) VipIMAGE 2017. ECCOMAS 2017. Lecture Notes in Computational Vision and Biomechanics, 27, Springer, Cham, 2018.
5. Cui Yiyao, Lv Xiaoshuo, Wang Feng, Kong Jie, Zhao Hao, Ye Zhidong, Si Chaozeng, Pan Lin, Liu Peng, Wen Jianyan, Geometry of the Carotid Artery and Its Association With Pathologic Changes in a Chinese Population, Frontiers in Physiology, 10, 2020.
6. M. Saqib Hameed, Awais Ahmad Shah, Muhammad Irfan Khan, Awais Ali, Imtiaz Hussain, Muhammad Dawood Bukhari, Comparison of blood flow analysis in stenosed and stented carotid artery bifurcation models, Cogent Engineering, 10(1), 2023.
7. Lopes D, Puga H, Teixeira J, Lima R. Blood flow simulations in patient-specific geometries of the carotid artery: A systematic review. J Biomech. 2020.
8. Mendieta JB, Fontanarosa D, Wang J, Paritala PK, McGahan T, Lloyd T, Li Z. The importance of blood rheology in patient-specific computational fluid dynamics simulation of stenotic carotid arteries. Biomech Model Mechanobiol, 19(5), 2020, 1477-1490.
9. Stamou AC, Radulovic J, Buick JM. A Comparison of Newtonian and Non-Newtonian Models for Simulating Stenosis Development at the Bifurcation of the Carotid Artery. Fluids. 8(10), 2023, 282.
10. Kumar, Nitesh, Khader, Abdul, Pai, R, Rao, D, Khan, Sanowar, k, Prakashini, Effect of Newtonian and non-Newtonian flow in subject specific carotid artery. Journal of Engineering Science and Technology, 15, 2020, 2764-2780.
11. Gharahi H, Zambrano BA, Zhu DC, DeMarco JK, Baek S. Computational fluid dynamic simulation of human carotid artery bifurcation based on anatomy and volumetric blood flow rate measured with magnetic resonance imaging. Int J Adv Eng Sci Appl Math, 8(1), 2016, 40-60.
12. Sacco S, Totaro R, Baldassarre M, Carolei A. Morphological variations of the internal carotid artery: Prevalence, characteristics and association with cerebrovascular disease. Int J Angiol. 2007 Summer;16(2):59-61.
13. Al-Sabbagh AA, Essa SI, Saleh AZ. A Comparative Study of the Right and Left Carotid Arteries in Relation to Age for Patients with Diabetes and Hypertension. Journal for Vascular Ultrasound, 46(3), 2022, 118-121.

14. Raja Rani T, Al Shibli A, Siraj M, Srimal W, Al Bakri NZS, Radhika TSL. ML-Based Approach to Predict Carotid Arterial Blood Flow Dynamics. Contemp. Math. 2023 Oct. 17. Available from: https://ojs.wiserpub.com/index.php/CM/article/view/3224
15. Raja Rani T, Srimal, W., Al Shibli, A., Al Bakri, N. Z. S., Siraj, M., & Radhika, T. S. L. (2023, October 10). Quantile Loss Function Empowered Machine Learning Models for Predicting Carotid Arterial Blood Flow Characteristics. Wseas Transactions on Biology and Biomedicine, 20, 155–170. https://doi.org/10.37394/23208.2023.20.16
16. Oshinski JN, Curtin JL, Loth F. Mean-average wall shear stress measurements in the common carotid artery. J Cardiovasc Magn Reson. 2006;8(5):717-22. doi: 10.1080/10976640600723839. PMID: 1689123
17. Sui B, Gao P, Lin Y, Gao B, Liu L, An J. Assessment of wall shear stress in the common carotid artery of healthy subjects using 3.0-tesla magnetic resonance. Acta Radiol. 2008 May;49(4):442-9. doi: 10.1080/02841850701877349. PMID: 18415789.
18. Liu Haipeng , Lan Linfang , Abrigo Jill , Ip Hing Lung , Soo Yannie , Zheng Dingchang , Wong Ka Sing , Wang Defeng , Shi Lin , Leung Thomas W. , Leng Xinyi, Comparison of Newtonian and Non-newtonian Fluid Models in Blood Flow Simulation in Patients With Intracranial Arterial Stenosis, Frontiers in Physiology, 12, 2021.
19. Gijsen FJ, van de Vosse FN, Janssen JD. The influence of the non-Newtonian properties of blood on the flow in large arteries: steady flow in a carotid bifurcation model. J Biomech. 1999 Jun;32(6):601-8.
20. D. Lopes, H. Puga, J.C. Teixeira, S.F. Teixeira, Fluid–Structure Interaction study of carotid blood flow: Comparison between viscosity models, European Journal of Mechanics - B/Fluids, 83, 2020, 226-234.
21. Min-Yi Lee, Chan-Ming Wu, Kuo-Ho Yu, Chih-Sheng Chu, Kun-Tai Lee, Sheng-Hsiung Sheu, Wen-Ter Lai, Association Between Wall Shear Stress and Carotid Atherosclerosis in Patients with Never Treated Essential Hypertension, American Journal of Hypertension, 22(7), July 2009, 705–710.